UCRL-JRNL-209355

LAWRENCE
LIVERMORE
NATIONAL
LABORATORY

Atomistic Simulation of Polymer Crystallization at Realistic Length Scales

R. H. Gee, L. E. Fried

February 2, 2005

Nature Materials

Disclaimer

This document was prepared as an account of work sponsored by an agency of the United States Government. Neither the United States Government nor the University of California nor any of their employees, makes any warranty, express or implied, or assumes any legal liability or responsibility for the accuracy, completeness, or usefulness of any information, apparatus, product, or process disclosed, or represents that its use would not infringe privately owned rights. Reference herein to any specific commercial product, process, or service by trade name, trademark, manufacturer, or otherwise, does not necessarily constitute or imply its endorsement, recommendation, or favoring by the United States Government or the University of California. The views and opinions of authors expressed herein do not necessarily state or reflect those of the United States Government or the University of California, and shall not be used for advertising or product endorsement purposes.

Atomistic Simulation of Polymer Crystallization at Realistic Length Scales

Richard H. Gee* and Laurence E. Fried

University of California
Lawrence Livermore National Laboratory
Chemistry and Materials Science Directorate
P.O. Box 808, L-268
Livermore, CA 94551

Understanding the dynamics of polymer crystallization during the induction period prior to crystal growth is a key goal in polymer physics.[1] Here we present the first study of primary crystallization of polymer melts via molecular dynamics simulations at physically realistic (about 46 nm) length scales. Our results show that the crystallization mechanism involves a spinodal decomposition microphase separation caused by an increase in the average length of rigid trans segments along the polymer backbone during the induction period. Further, the characteristic length of the growing dense domains during the induction period is longer than predicted by classical nucleation theory.[2] These results indicate a new "coexistence period" in the crystallization, where nucleation and growth mechanisms coexist with a phase separation mechanism. Our results provide an atomistic verification of the fringed micelle model.

* To whom correspondence should be addressed.

Understanding the crystal nucleation and growth processes in polymeric materials is one of the most important grand challenges in the field of polymer physics. Understanding the mechanism of polymer crystallization is a key to understanding the material properties of semicrystalline polymers.

Since the discovery[3] that flexible macromolecular chain molecules organize into thin, lamellar crystals separated by an amorphous matrix, the polymer physics community has grappled with both the nucleation process and the ensuing structure of the material. Considerable progress has been made in our molecular level understanding of the crystallization process, structure and properties of these materials through both experimental[4] and theoretical[5-9] efforts. These studies have focused mainly on crystal nucleation and growth, where it is generally understood that critical nuclei are formed from a metastable state during the first stages of crystallization leading ultimately to nucleation and growth. Thus, randomly coiled chain molecules must transform into nuclei with a regular lattice from which growth takes place at the growth front. However, relatively little is known about the structure formation during the so-called induction period before crystal nucleation.

Recently, much attention has been given to the precursory structure during the crystallization induction period.[1, 10-15] Recent work has revealed a pretransition state which occurs prior to crystallization. This pretransition state has been characterized as a spinodal decomposition phase separation initiated by orientational fluctuations caused by

an increase of rigid rod-like segments. Specifically, a scattering peak corresponding to density fluctuations has been observed in the time resolved small-angle x-ray scattering (SAXS) measurements during the induction period.[1, 10-15] These observations are consistent with the theory proposed by Doi *et al.*[16] on the isotropic-to-nematic transition of polymer liquid crystals; i.e., parallel ordering of polymer chain molecules are caused by an increase in chain rigidity. Experimental measurements have confirmed this.[1]

Much of the theoretical work put forth towards the understanding of polymer crystallization has made use of molecular dynamics (MD) simulations[6, 9, 17-19] because of the atomistic detail that MD provides. To this end, we use MD to study the primary nucleation process of entangled amorphous melts of bulk pVDF at realistic length scales (where the length scales used here allow for direct resolution of the large-wavelength fluctuations associated with spinodal decomposition as well the experimental length scales of the polymer microstructure), using a united-atom (UA) polymer model[20] consisting of 8,640 120-mer polymer chains (2,073,600 total united-atoms; giving a periodic cell dimensions of ~46 nm). In order to induce crystallization, the bulk system was rapidly cooled using the protocol outlined in the Appendix. This distinguishes our work from prior studies, where secondary nucleation was induced at a surface,[9] or where the simulation cell was insufficiently large to resolve spinodal decomposition.[6, 21] Here we focus mainly on this induction period. Our simulations show a microphase separation from the amorphous melt phase into a semicrystalline polymer with multiple crystal domains (see Fig. 1). The intermolecular order found in the polymer

microstructure is equivalent to the well-known β-pVDF polymorph, which has an orthorhombic unit cell.

Further, our results show peaks in the time dependent structure factor *S(q,t)*, resulting from the lamellar repeat or long period peak (q≈0.065 $Å^{-1}$; d≈100 Å) as well as a peak at lower *q* values corresponding to the induction peak (q≈0.04 $Å^{-1}$; d≈160 Å), which is indicative of parallel ordering of sections of polymer chains during the induction period before the onset of primary crystallization, as shown in Fig. 2*a*. The positions of the induction and long period peaks found here are similar to those found experimentally[22] for the spinodal-assisted crystallization. This indicates that we have achieved a molecular simulation on a physically realistic length scale. Both peaks in the simulation are readily apparent early on in the simulation after the polymer melt is quenched to a temperature below the melt temperature and are shown to grow with time, similar to experiment[1, 14, 15] (see Fig. 2). As is evident from Fig. 2*a*, the induction peak and the long period peak appear simultaneously, and grow at a similar rate early in the simulation. At longer times, the structure due to the long period peak becomes more pronounced and over-runs the induction peak. Additionally, the time dependence of the peak in *S(q,t)* corresponding to the nearest-neighbor packing (second-order Bragg peak) shows a prominent shift from unoriented domains (q ≈ 1.06 $Å^{-1}$; d ≈ 5.9 Å) to segment-oriented domains (q ≈ 1.19 $Å^{-1}$; d ≈ 5.3 Å) at around ~10 ns (see Fig. 2*a* inset), which coincides

with the stagnation of the induction peak (see discussion below). This shift corresponds to the nematic to smectic phase transition, similar to polymer liquid crystals.

The existence of the induction peak in Fig. 2*a* suggests that the mechanism of primary crystal nucleation is spinodal decomposition. Evidence of a spinodal-assisted crystallization process can be found by analyzing the time dependent structure factor *S(q,t)* during the early stages of the crystallization process in terms of the Cahn-Hilliard[23] theory for spinodal decomposition. According to this theory, a fluid undergoing a demixing instability will experience fluctuations in composition that grow exponentially, of the form

$$S(q,t) \propto S(q,0)\exp[2R(q)t], \tag{1}$$

where *R(q)* is the wavevector-dependent growth rate at a given *q*. The spinodal-assisted signature is that the so-called Cahn plot [$R(q)/q^2$ versus q^2] should exhibit linear behavior with a negative slope. The Cahn plot of our simulation results in Fig. 2*b* illustrates typical spinodal-assisted behavior for the early stages of the crystallization process. The solid line is a fit to the data. This type of behavior is indicative of a spinodal-type growth mechanism and is attributed to the early-stage generation of rigid segments in the polymer.[1] To elucidate the length at which the rigid chain segments become critical, causing the microphase separation, the average segment length, (average number of consecutive *trans* conformers) along the polymer backbone (these segments coinciding to the rigid chain segments referred to in Doi's[16] theory) were monitored as a function of time throughout the simulation. The integral of *S(q,t)* in certain *q* regions is

also calculated so as to further quantify the structural evolution of *S(q,t)*. Fig. 3*a* shows the average segment length, and the integrated *S(q,t)* intensity of both the induction peak ($q \approx 0.027$-0.05) and the long period peak ($q \approx 0.05$-0.1). It is readily apparent that peak structure emerges early on in the simulations, within ~5 ns after quenching below the melt transition temperature. The rapid emergence of structure seen here is directly related to the sudden cooling employed and the significant degree of undercooling in the simulations (see below), since the rate of crystallization is the result of a balance between the molecular mobility, which increases with temperature above T_g and the driving force for crystallization, which increases with undercooling. Thus, our simulated polymer ensemble is quenched significantly below the equilibrium melting point, and crosses the spinodal associated with the buried liquid-liquid bimodal inside the equilibrium liquid-crystal coexistence region.[7] This provides a plausible explanation for the spinodal-assisted phase separation seen here. The initial emergence of the induction and long period peak structure coincides with an average segment length (rigid polymer segments) of ~12-15 Å, which may be thought of the critical size of the initiatory crystal nuclei appearing in the dense domains. The size of the critical nuclei determined here, are consistent with the size determined from experiment.[22] Between 5 and 10 ns the induction peak grows more rapidly than the long period peak. During this period, both spinodal decomposition and crystallite growth are occurring at the same time. After 10 ns the long period peak dominates and the induction peak stagnates. The point at which the induction peak no longer grows ($t \approx 10$ ns) indicates the end of the precursory induction period, and thus the phase transition from nematic to smectic, similar to polymer liquid crystals. It is

at this point that growth takes place at the newly formed crystallite growth front, as in classical nucleation theory.[2] This suggests that the underlying nucleation mechanism requires rigid chain segments of a critical average length (~12-15 Å). Above this length the system becomes unstable in order to reduce the excluded volume, the rigid segments are forced to orient parallel to one another, leading to density fluctuations caused by the oriented and unoriented domains. This is further evidence of a spinodal decomposition, where oriented and unoriented domains coexist.[16] Namely, the spinodal decomposition differs from the classical nucleation and growth of polymer crystallization in that the spinodal decomposition occurs when the melt is quenched well below the metastable liquid-liquid coexistence boundary into the unstable region of the hidden liquid-liquid boundary.[7] The oriented and unoriented domains are analogous to nematic and isotropic phases in liquid crystals, respectively, where the oriented phase (nematic phase) contains many entanglement points. As the nucleation proceeds, the oriented domains further separate into smectic and amorphous phases, resulting in an alternating smectic and amorphous structure which gives rise to the observed long period peak in $S(q,t)$, as seen here. Finally, the prominent shift in the second-order Bragg peak shown in the inset in Fig. 2*a* is further elucidated by monitoring the Bragg spacing as a function of time (Fig. 3*b*, where the Bragg peak stops shifting at ~25 ns into the simulation. The average polymer segment length at the point in which the Bragg spacing shifts is ~70 Å, and may be thought of as the critical thickness before parallel chain ordering can be realized. The critical thickness calculated here compares well with the experiments.[22]

Many attempts have been made to explain polymer crystallization in term of the fringed micelle model,[24, 25] where it is assumed that during crystallization some regions of the polymer melt align and form bundles of parallel chain segments which grow laterally by aggregation of rigid segments, where entanglements ultimately prevent complete crystallization. However, controversy still exists as to whether melt crystallized polymer materials crystallize into regularly folded chain lamellae or fringed micelle**s**[1, 25]**.** This is a basic question of whether the crystallization process is a chain folding process unique to long chain macromolecules or a process of lateral cohesion of chain segments similar in nature to the crystallization of other molecular solids.

The overall morphology obtained here is a "fringed micelle" (see Fig 4), where regularly packed (aligned) crystalline regions are randomly dispersed in an amorphous matrix. The lamellae are dispersed within a granular texture consisting of crystallite regions of ~100 Å in size separated by amorphous material. Further, since the polymer chain length is much longer than the average crystallite dimension, the polymer chains pass from one crystallite through an amorphous area, back into another crystallite (see Fig. 4*b*). Additionally, there is no overall directionality to the formed lamellae. Granular features like those in Figure 4 have been identified experimentally[26], and have been attributed to microphase separation.

Our results support a fringed micelle morphology induced by a spinodal decomposition phase separation. Finally, our analysis of the pVDF microstructures studied here display

local density and orientational order fluctuations precursory to the onset of primary polymer crystal nucleation suggesting thermodynamic instability due to the *rapid* quench below the metastable liquid-liquid coexistence boundary into the unstable region of the hidden liquid-liquid boundary. Our analysis suggests a spinodal-assisted crystallization process. Nucleation is brought about as a result of reduced thermal motion, increased density, and extended chain conformations along the polymer chain backbone. This suggests that the strong coupling between the chain conformation and density is a driving force in polymer crystallization. The nucleation process during the induction period occurs via a three-stage process, consisting of first, an extended trans sequence formation stage (decrease in conformational entropy), second, cluster formation or lateral cohesion stage, and third, a growth stage. The pre-ordering phase (stage one) identified here seems to be equivalent to the ordering proposed by Imai *et al.,*[1] using x-ray scattering experiments. The onset of the extended trans sequence formation stage (rigid segments) occurs extremely rapidly, during the induction period, once the ensemble is quenched into the unstable region of phase space. Our results indicate a new "coexistence period" in the crystallization, where nucleation and growth mechanisms are concomitant with spinodal phase separation mechanism. We also demonstrate that molecular studies of polymer crystallization at physically realistic length scales are now possible with massively parallel computational resources.

Methods

Polymer Model

The MD simulations of polar polymer melts were carried out on a bulk amorphous ensemble composed of 8,640 120-mer polymer chains (2,073,600 united-atoms; M_w=7682 g/mol). The UA polymer model represents a VDF polymer analogue, where the hydrogen or fluorine atoms are lumped onto the carbon backbone atoms to which they are attached; $-CH_2-$ replaced by a single bead with a, mass of 14 amu's or $-CF_2-$ replaced by a single bead with a mass of 50 amu's). The simplified UA model affords the investigation of much larger polymer ensemble, reducing finite size effects, due to the substantial increase in simulation times accessible. The initial starting polymer configurations for simulations in the bulk were generated using a Monte Carlo method. The monomers were allowed to 'polymerize' in a head-to-tail manner with no monomer reversals. The initial atomic positions of the amorphous melt structure were generated using a random distribution of torsional angles, which was generated using a Monte Carlo method that assigns random values to all rotatable torsions in the polymer chain. The resulting amorphous structure was then relaxed by energy minimization.

The MD simulations of bulk UA pVDF melts employed the force field parameter set of Gao *et al.*.[20] The UA polymer model is consists of both valence (bond, angle, and torsion terms) and nonbonded potential terms (vdW and Coulomb). All valence degrees of freedom were explicitly treated and unimpeded.

Appendix: Molecular Dynamics Method

The amorphous polymer structures were simulated using 3-dimensional cubic periodic boundary conditions. The simulations were generated using constant particle number,

pressure, and temperature (*NPT)* dynamics at a pressure of 0 atm. All computations were carried out using LAMMPS (large-scale atomic/molecular massively parallel simulator) code.[27] The equations of motion were integrated using the Verlet algorithm[28] with a time step of 2.0 fs for temperatures above the onset temperature of crystallization (600 K) and 4 fs at 600 K. A Nose-Hoover-type thermostat[29] with a relaxation time of 0.1 ps was used to control the temperature, and the pressure was controlled isotropically.[30] The Lennard-Jones potential parameters for the van der Waals interaction of heterogeneous atomic pairs were calculated from the geometric mean of parameters of each atom. Further, the nonbonded van der Waals interactions were treated by truncating atom pairs with an inter-atomic distance greater than 12 Å. The particle-particle particle-mesh Ewald (PPPM) method[31] (accuracy criterion was set to $1x10^{-5}$ and the near-field cutoff to 10.0 Å) was used for the long-range treatment of electrostatic interactions.

The ensemble was initially simulated at 750 K. The periodic box was allowed to relax under *NPT* conditions. The volume equilibration process was carried out for a minimum duration of 5 ns. Following this step, the ensemble was cooled in *NPT* runs in increments of 50 K and equilibrated for a minimum of 5 ns each at the desired temperature (750 K, 700 K, and 650 K). At a temperature of 600 K (the temperature at which the polymer nucleates) the simulations were carried out for more than 30 ns.

Acknowledgements

The work was performed under the auspices of the U.S. Department of Energy by the University of California Lawrence Livermore National Laboratory under Contract W-7405-Eng-48.

FIGURES

Figure 1. Snapshots from the MD simulations showing the evolution of the spinodal-assisted crystallization process at a temperature of 600 K. Only the oriented domains (OD) are explicitly shown (the unoriented amorphous domains (UOD) are the white space in each panel). The times associated with the evolution in each of the panels *a-f* are 2, 4, 6, 8, 10, 31.2 ns, respectively.

Figure 2. Time dependent structure factor, *S(q,t)* at 600 K. Panel *(a)* shows both the induction peak ($q \approx 0.04$ Å^{-1}; d≈160 Å) corresponding to phase separation domains and the long period peak ($q \approx 0.065$ Å^{-1}; d≈100 Å) corresponding to lamellar distances. The inset in panel *(a)* shows the second-order Bragg peak in *S(q,t)*; where the transition from unoriented to oriented packing is readily apparent. The times associated with each of the curves in panel (*a*), and the inset, are 0.08, 3.28, 6.56, 9.84, 13.44, 15.12, 15.52, 21.44, 21.84, and 31.2 ns, from the bottom curve to the top curve, respectively. Panel (*b*) shows the Cahn-Hilliard plot derived from the early stages of the nucleation process in the polymer crystallization simulations at 600 K. The linear nature of the plot demonstrates the presence of a spinodal-assisted crystallization process.

Figure 3. The time evolution of the average segment length, $\langle l_s \rangle$ (dotted curve) and integrated intensity of the low-angle scattering peak [*S(q,t)* integrated for $q \approx 0.027$-0.05 (grey curve) and $q \approx 0.05$-0.1 (solid curve)] is shown in panel (*a*). The induction peak in *S(q,t)* is shown to be slightly more pronounced in the early stages of nucleation (5-10 ns) and then ceases to grow after ~15 ns, while the intensity associated with the long period peak continues to increase throughout the entire simulation. Panel (*b*) shows the time evolution of the second-order Bragg peak location, converted to an effective interchain distance d. The shift at ~10 ns corresponds to the nematic to smectic phase transition.

Figure 4. Panel *(a)***:** representative polycrystalline ensemble of pVDF at 600 K showing a "fringed-micelle" type morphology. Panel *(b):* a small segment of the entire polymer ensemble showing both regularly packed and randomly dispersed amorphous regions, where the crystal folds consist of sharp regular folds, long and short loops and cilia. Individual polymers are colored to illustrate polymer chains entering the amorphous region from an ordered region, and adjoining two separate adjacent crystallites (adjacent crystallites not explicitly shown). Panel *(c):* a two-dimensional cartoon of the fringed-micelle model used to explain crystalline polymers.

References and Notes

1. Kaji, K., Nishida, K., Matsuba, G., Kanaya, T. & Imai, M. Details of Structure Formation During the Induction Period of Spinodal-Type Polymer Crystallization. Journal of Macromelecular Science-Physics B42, 709-715 (2003).
2. Frenkel, I. I. The Kinetic Theory of Liquids (Clarendon, Oxford, 1946).
3. Keller, A. A Note on Single Crystals in Polymers: Evidence for a Folded Chain Configuration. Philos. Mag. 2, 1171-1175 (1957).
4. Yau, S.-T. & Vekilov, P. G. Quasi-planar nucleus structure in apoferritin crystallization. Nature 406, 494 (2000).
5. Oxtoby, D. W. Phase transitions: Catching crystals at birth. Nature 406, 464 (2000).
6. Gee, R. H. & Fried, L. E. Ultrafast crystallization of polar polymer melts. J. Chem. Phys. 118, 3827 (2003).
7. Olmsted, P. D., W.C.K.Poon, McLeish, T. C. B., Terrill, N. J. & A.J.Ryan. Spinodal-Assisted Crystallization in Polymer Melts. Physical Review Letters 81, 373 (1998).
8. ten Wolde, P. R. & Frenkel, D. Enhancement of protein crystal nucleation by critical density fluctuations. Science 277, 1975 (1997).
9. Yamamoto, T. Molecular dynamics modeling of polymer crystallization from the melt. Polymer 45, 1357-1364 (2004).
10. Strobl, G. R. The Physics of Polymers (Springer-Verlag, Berlin, 1996).
11. Cakmak, M., Teitge, A., Zachmann, H. G. & White, J. L. Online small-angle and wide-angle x-ray-scattering studies on melt-spinning poly(vinylidene fluoride) tape using synchrotron radiation. J. Polymer Science Part B: Polymer Physics 31, 371-381 (1993).
12. Terrill, N. J. et al. Density fluctuations: the nucleation event in isotactic polypropylene crystallization. Polymer 39, 2381-2385 (1998).
13. Kimura, T., Ezure, H., Tanaka, S. & Ito, E. In situ FTIR spectroscopic study on crystallization process of isotactic polystyrene. J. Polym. Sci., B 36, 1227-1233 (1998).
14. Heeley, E. L. et al. Early stages of crystallization in isotactic polypropylene. Macromolecules 36, 3656-3665 (2003).

15. Matsuba, G., Kaji, K., Kanaya, T. & Koji, N. Detailed analysis of the induction period of polymer crystallization by depolarized light scattering. Phys. Rev. E 65, 061801 (2003).

16. Shimada, T., Doi, M. & Okano, K. Concentration fluctuation of stiff polymers. III. Spinodal decomposition. J. Chem. Phys. 88, 7181 (1988).

17. Muthukumar, M. & Welch, P. Modeling polymer crystallization from solutions. Polymer 41, 8833-8837 (2000).

18. Takeuchi, H. Structure formation during the crystallization induction period of a short-molecule system: A molecular dynamics study. J. Chem. Phys. 109, 5614-5621 (1998).

19. Hu, W., Frenkel, D. & Mathot, V. B. F. Intramolecular Nucleation Model for Polymer Crystallization. Macromolecules 36, 8178-8183 (2003).

20. Gao, G. (California Institute of Technology, 1998).

21. Meyer, H. & Muller-Plathe, F. Formation of Chain-Folded Structures in Supercooled Polymer Melts Examined by MD Simulations. Macromolecules 35, 1241-1252 (2002).

22. Imai, M., Kaji, K. & Kanaya, T. Structural Formation of Poly(ethylene terephthalate) during the Induction Period of Crystallization. 3. Evolution of Density Fluctuations to Lamellar Crystal. Macromolecules 27, 7103 (1994).

23. Cahn, J. W. & Hilliard, J. E. Free energy of a nonuniform system I. Interfacial free energy. J. Chem. Phys. 28, 25 (1958).

24. Herman, K., Gerngross, O. & Abitz, W. X-ray studies of the structure of gelatin micelles. Z. Phys. Chem 10, 371 (1930).

25. Flory, P. J. On the Morphology of the Crystalline State in Polymers. J. Amer. Chem. Soc. 84, 2857 (1962).

26. Bensason, S. et al. Classification of Homogeneous Ethylene-Octene Copolymers Based on Comonomer Content. Journal of Polymer Science: Part B: Polymer Physics 34, 1301-1315 (1996).

27. Plimpton, S. J. Fast Parallel Algorithms for Short-Range Molecular Dynamics. J. Comp. Phys. 117, 1-19 (1995).

28. Verlet, L. Computer "Experiments" on Classical Fluids. I. Thermodynamical Properties of Lennard-Jones Molecules. Phys. Rev. 159, 98 (1967).

29. Nose, S. A unified formulation of the constant temperature molecular dynamics methods. J. Chem. Phys. 81, 511 (1984).

30. Melchionna, S., Ciccotti, G. & Holian, B. L. Hoover's style Molecular Dynamics for systems varying in shape and size. Mol. Phys. 78, 533 (1993).

31. Hockney, R. W. & Eastwood, J. W. Computer Simulation using Particles (McGraw-Hill, New York, 1981).

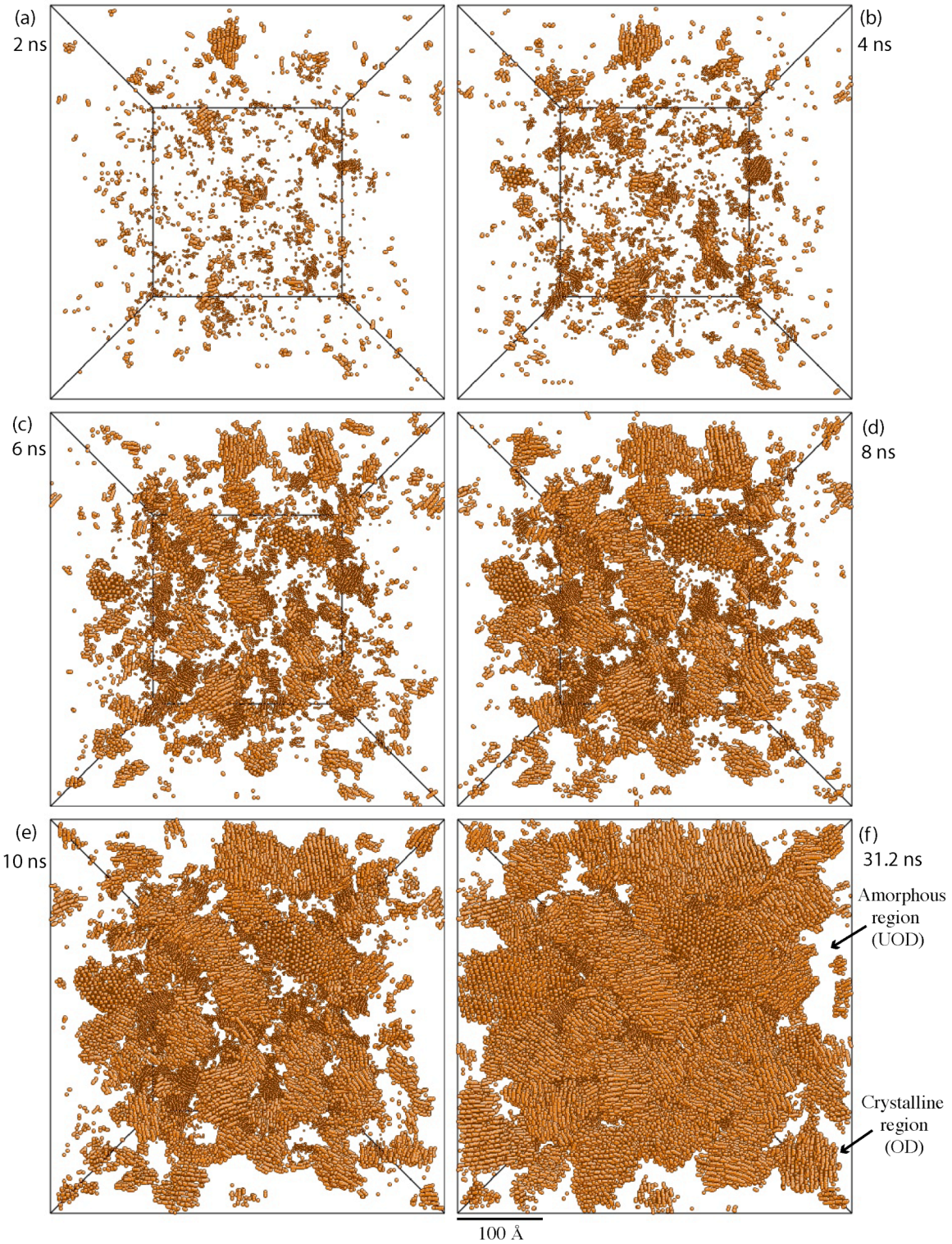

Figure 1. R. Gee *et al.*

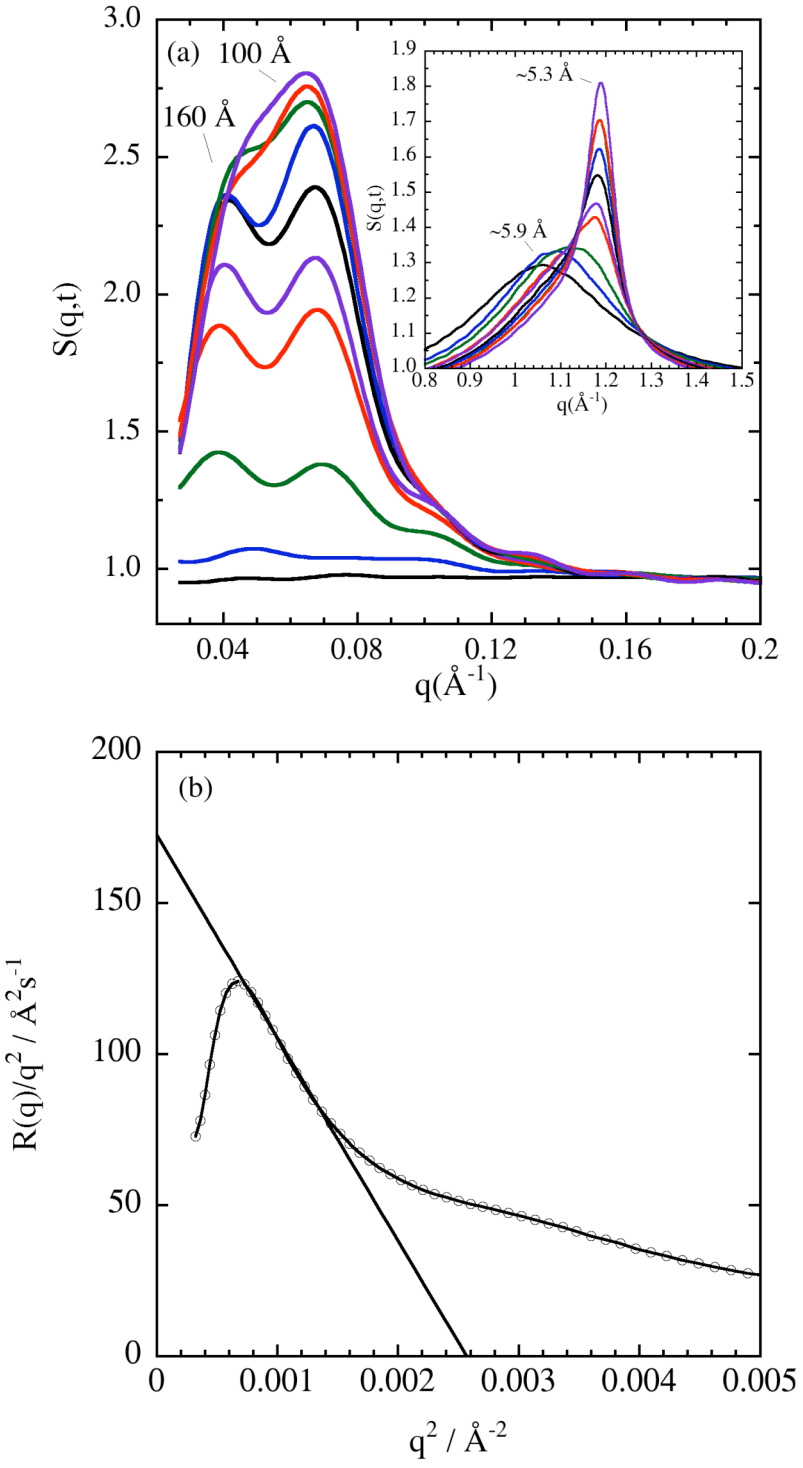

Figure 2. R. Gee *et al.*

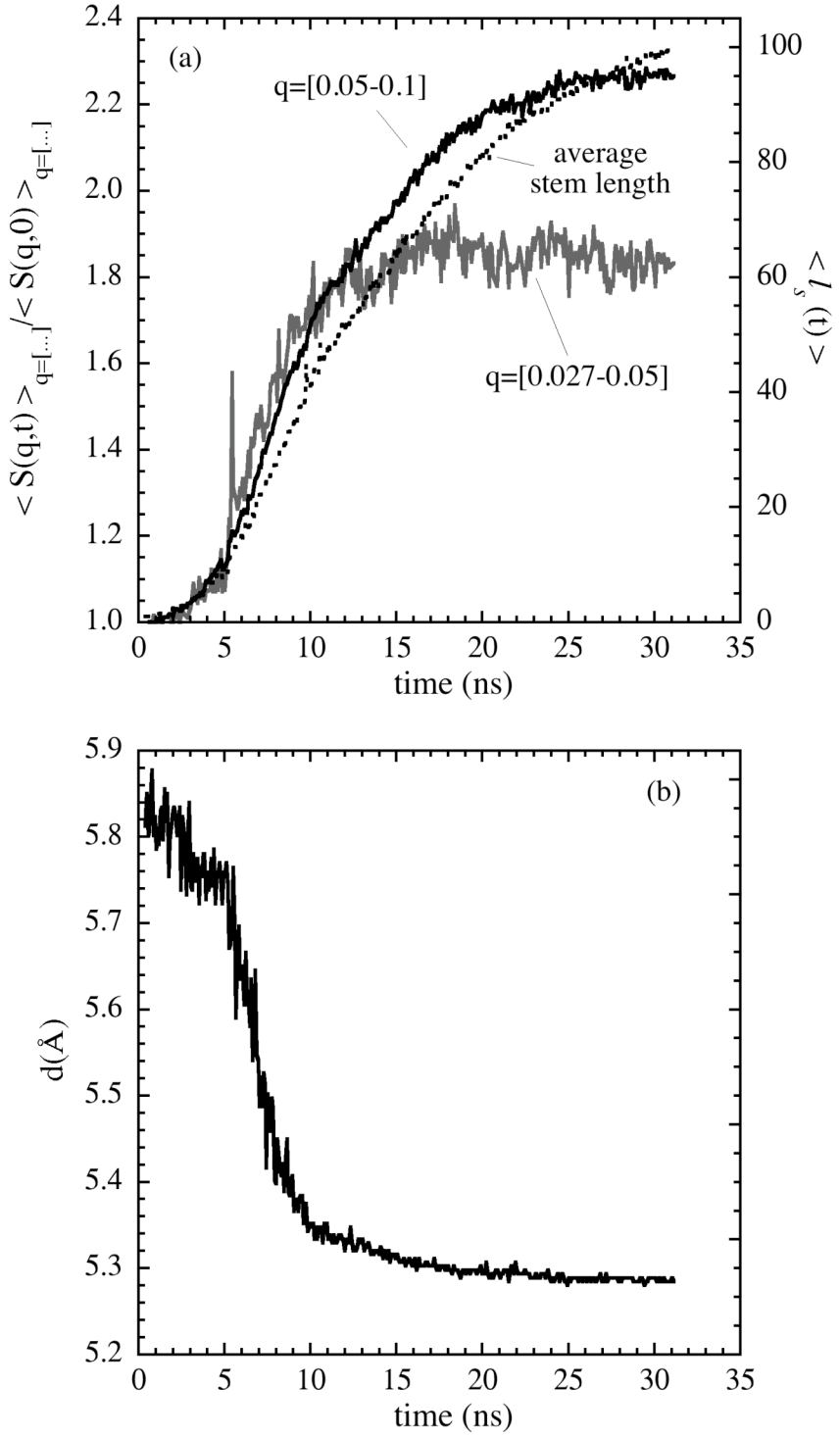

Figure 3. R. Gee *et al.*

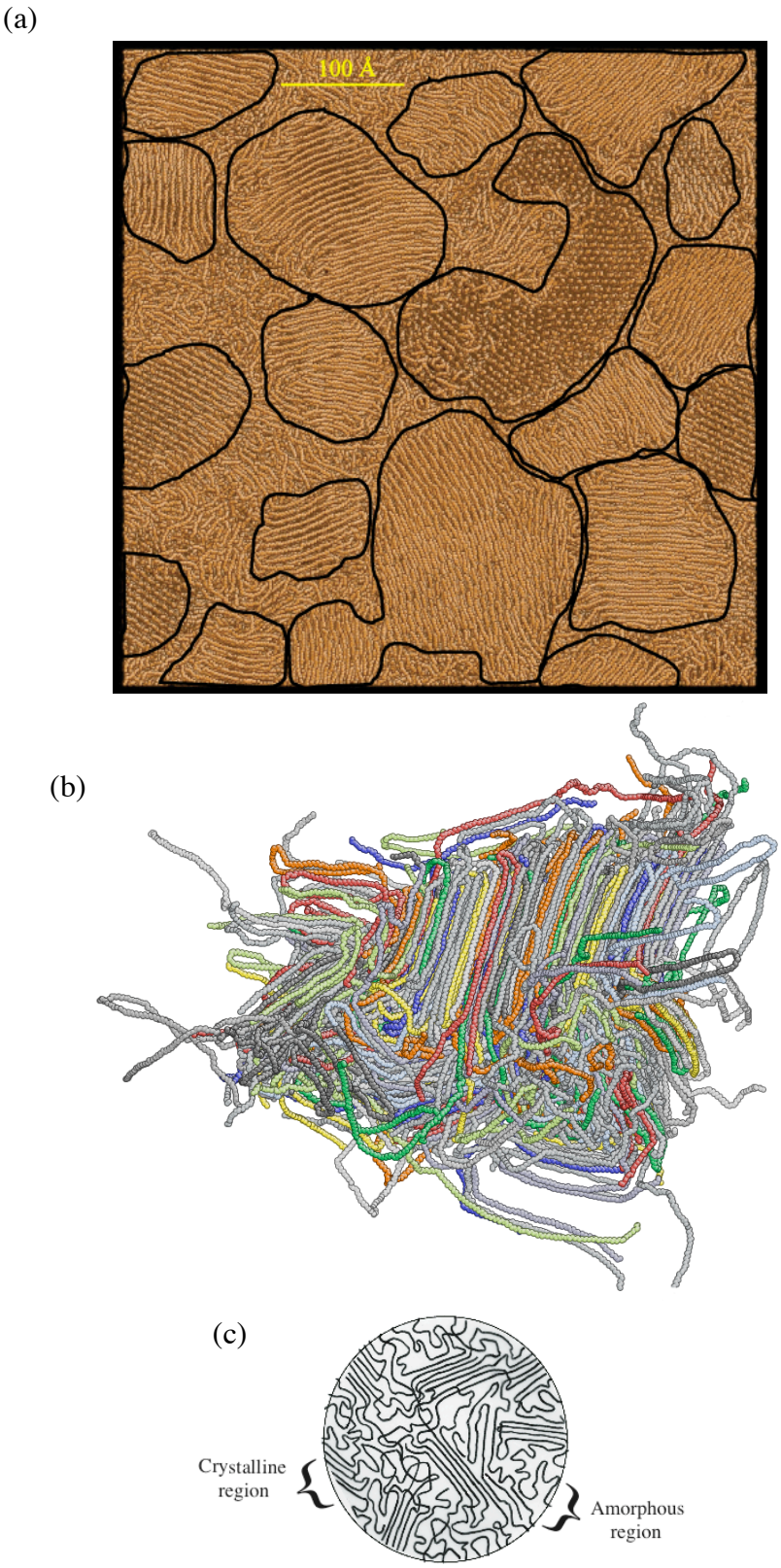

Figure 4. R. Gee *et al*.